Generalized theory of smallest diameter of metallic nanorods

Feng Du, Paul R. Elliott, and Hanchen Huang*

Department of Mechanical and Industrial Engineering, Northeastern University, Boston, Massachusetts 02115, USA

(Received 28 March 2017; revised manuscript received 21 June 2017; published 9 August 2017)

This paper reports a generalized theory of the smallest diameter of metallic nanorods from physical vapor deposition. The generalization incorporates the effects of nanorod separation and those of van der Waals interactions on geometrical shadowing. The generalized theory relies on approximations to be in closed form. Numerical solutions of governing equations with no approximations verify the accuracy of the closed-form theory. Further, experiments of physical vapor deposition validate the theory in terms of the diameter as a function of the separation of nanorods. In contrast, the previous theory for idealized geometrical shadowing [X. B. Niu *et al.*, Phys. Rev. Lett. **110**, 136102 (2013)] excludes any dependence on nanorod separation and predicts the diameter to be about ½ to ⅓ of what the generalized theory does.

DOI: 10.1103/PhysRevMaterials.1.033401

I. INTRODUCTION

The diameter of metallic nanorods from physical vapor deposition (PVD) is a critical quantity that defines their functionalities, such as mechanical strength [1–3] and sensitivity in surface-enhanced Raman spectroscopy [4–6]. Conventional PVD processes typically lead to the growth of thin films [7,8]. Under glancing angle deposition (GLAD), PVD processes result in the growth of nanorods [9,10]. As atoms arrive on a substrate with a glancing angle that is close to 90°, they land at peaks and avoid valleys due to geometrical shadowing effects. As an effect of positive feedback, the peaks grow into nanorods due to geometrical shadowing. In the processes of nanorod growth, multiple-layer surface steps form and impose three-dimensional (3D) Ehrlich-Schwoebel (ES) barriers [11,12] that are larger than the conventional ES barriers from monolayer surface steps [13,14].

The diameter of nanorods is the smallest when the 3D ES barriers dominate or, equivalently, when multiple-layer surface steps bound the top of nanorods [15] under a given geometrical shadowing condition. The geometrical shadowing goes to complete, or ideal, as the incidence angle approaches 90°. Under this idealized condition, all atoms will be deposited on the top surface of nanorods with none reaching their side surfaces, independent of nanorod separation. For such idealized geometrical shadowing, we recently reported a closed-form theory of the smallest diameter [15].

Going beyond the idealized shadowing condition, here we report a generalized theory, in closed form, with nonideal shadowing conditions and with the effects of van der Waals (vdW) interactions. Figure 1 schematically illustrates the generalization of a nanorod growth process. The direct deposition on the top results in a diameter of the core (orange in Fig. 1), which is governed by our previous theory [15]. The deposition on the sides gives the thickness of the shell (tan in Fig. 1) and it depends on the separation of nanorods. Further, due to vdW interactions, the atomic flux on the top is greater than on the side of nanorods, as indicated by the denser flux lines in Fig. 1.

Conceptually, the top surface of a nanorod advances at a rate that is higher than the deposition rate because of the denser flux lines; the amount of diffusion off the top surface and down the sides is small, as shown previously [15]. Further, under quasi-steady-state growth, the diameter of the nanorods is dictated by (1) its vertical growth rate, which is the rate that its top surface advances, and (2) the total amount of atoms it receives, which depends on the nanorod separation.

In the following, we first derive the closed-form theory of the flux on the top of nanorods to account for the vdW interactions, then use this theory to derive a generalized theory of nanorod diameter that is also in closed form. Following the formulation of the generalized theory, we carry out numerical calculations to verify the theory and PVD experiments to validate the theory.

II. THEORY AND VERIFICATION

As the first step of formulating the expression of effective deposition flux to account for the vdW interactions, we consider a system consisting of an incoming atom and a large flat substrate. As shown in Fig. 2, an incoming atom on the x-z plane has a velocity of magnitude V_0 and a direction that forms angle θ with z. Due to vdW interactions, its trajectory deviates from the straight broken line to the curved solid line. Although the vdW interaction between two atoms decays with the sixth power of distance, the interaction between an atom and a large flat surface (or semi-infinite solid) decays with the third power of distance. For the system in Fig. 2, the interaction energy $E(z)$ is $-C/z^3$ [16–18]. For copper-copper interactions, as the prototype in this paper, a typical value of C is 2.1×10^{-3} eV nm^3 [19]. In PVD processes, the distance between substrate and source is of the order of a fraction of a meter. The interaction energy at such a large distance is practically zero. As the atom approaches the surface, energy conservation leads to the following equation of motion:

$$\frac{dz}{dx} = -\frac{\sqrt{\frac{2C}{mz^3} + V_0^2 \cos^2\theta}}{V_0 \sin\theta}, \tag{1}$$

where m and V_0 are the mass and the initial speed of the atom, respectively.

*Author to whom correspondence should be addressed: h.huang@northeastern.edu

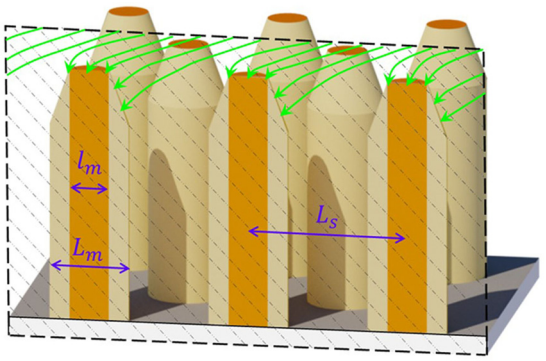

FIG. 1. Schematic of nanorod growth, showing atomic flux (green lines) in a vertical cross section that cuts through the center of three nanorods in the front.

In order to achieve a closed-form theory, we consider two segments of the trajectory using approximations. In one segment, the initial kinetic energy is relatively larger in magnitude than the vdW interaction energy. As an approximation, the equation becomes

$$\frac{dx}{dz} = -\tan\theta\left(1 - \frac{C}{mz^3V_0^2\cos^2\theta}\right). \tag{2}$$

In the absence of the vdW interactions, the equation of motion is

$$\frac{dx}{dz} = -\tan\theta. \tag{3}$$

The lateral distance traveled by the atom according to Eq. (2) is smaller than that according to Eq. (3) by amount Δ_1, which is also shown in Fig. 2. From Eqs. (2) and (3), we have

$$\frac{d\Delta}{dz} = \frac{C\sin\theta}{mz^3V_0^2\cos^3\theta}. \tag{4}$$

As the atom arrives at a vertical distance z_c,

$$\Delta_1 = \frac{C\sin\theta}{2mz_c^2V_0^2\cos^3\theta}. \tag{5}$$

In the other segment of the trajectory, the vdW interaction energy is larger than the initial kinetic energy in magnitude. As an approximation, Eq. (1) becomes

$$\frac{dz}{dx} = -\frac{1}{V_0\sin\theta}\sqrt{\frac{2C}{mz^3}}. \tag{6}$$

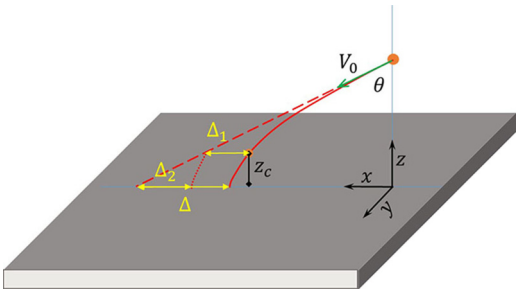

FIG. 2. Schematic of trajectory deviation of an incoming atom toward a flat substrate by Δ, due to vdW interactions.

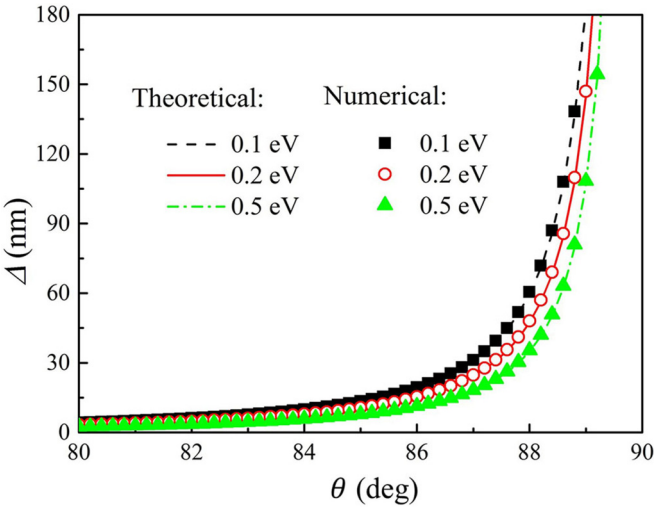

FIG. 3. Comparison of closed-form theory of Eq. (9) with numerical solutions of Eq. (1), as a function of angle θ and initial kinetic energy of the incoming atom.

As the atom travels from vertical position z_c to $z = 0$, the lateral distance it travels according to Eq. (6) is smaller than that according to Eq. (3) by the amount Δ_2, as shown in Fig. 2:

$$\Delta_2 = z_c\tan\theta - \frac{2}{5}V_0\sin\theta z_c^{\frac{5}{2}}\sqrt{\frac{m}{2C}}. \tag{7}$$

We choose z_c to be the point when the vdW interaction energy and the initial kinetic energy due to vertical motion (that is, $mV_0^2\cos^2\theta/2$) are equal in magnitude. As a result of this choice,

$$z_c = \left(\frac{2C}{mV_0^2\cos^2\theta}\right)^{\frac{1}{3}}. \tag{8}$$

The sum of Δ_1 and Δ_2 approximately describes how much the trajectory of an atom is deflected:

$$\Delta = \Delta_1 + \Delta_2 = \tfrac{17}{20}z_c\tan\theta. \tag{9}$$

To verify the approximate expression of Eq. (9), we also numerically solve Eq. (1). As shown in Fig. 3, the approximate expression is accurate for glancing angles beyond 80° and for typical kinetic energies around 0.2 eV [16,20–22]; below 80°, the deflection becomes unimportantly small. It is important to note that the deflection can be as large as 100 nm, which is comparable to typical diameters and separations of nanorods and is therefore consequential for the growth of nanorods.

Having established the closed-form theory of deflection on a flat substrate and verified its accuracy, we next extend the theory to more realistic cases of nanorods in three dimensions. To obtain a closed-form theory, we consider a tall and isolated nanorod, as shown in Fig. 4. For this system, the vdW interaction energy E is primarily from the interaction between the incoming atom and the nanorod, as opposed to between the nanorod and the substrate, and is given by

$$E(x,y,z) = \iiint \frac{-\rho C_6}{r^6}dW, \tag{10}$$

where r is the distance between the incoming atom and the volume element dW of the nanorod, and ρ is the density of

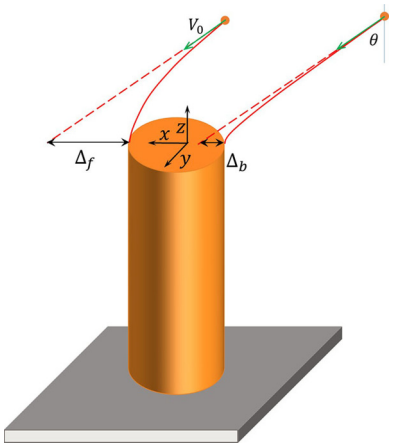

FIG. 4. Schematic of the trajectory deviation of an incoming atom toward a nanorod, due to vdW interactions, from two initial locations.

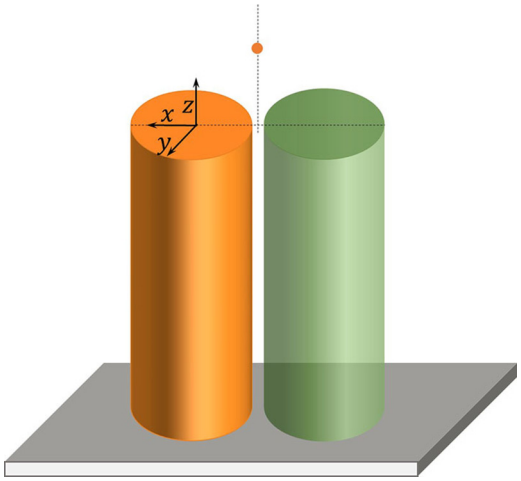

FIG. 5. Approximate representation of the vdW interaction between an atom and nanorod when the atom approaches the nanorod surface.

the nanorod. The interaction constant C_6 scales with C, and for face-centered-cubic materials, $\rho C_6 = 6C/\pi$.

Based on the principle of energy conservation, we have an equation of motion similar to Eq. (1). In order to achieve a closed-form theory, we note that the vdW interactions are the most effective only when the atom is in close proximity to the top surface of the nanorod, and further the strongest interactions come from the volume elements of the nanorod that are immediately below the atom. Therefore, instead of using the nanorod in Fig. 1, we use only the core of the nanorod as shown in Fig. 4. As an approximation in deriving the front deflection Δ_f, the interaction energy between an atom and the nanorod is

$$E(x,y,z) \approx E(0,0,z). \tag{11}$$

Since the core diameter l_m is typically much larger than a nanometer, $l_m \gg z$ when the interactions are strong. Therefore, Eq. (11) approximately becomes

$$E_{l_m \gg z}(0,0,z) = -\frac{C}{z^3}\left(1 - \frac{6\pi z^3}{l_m^3}\right). \tag{12}$$

The critical height z_{cn}, at which the kinetic energy and the vdW interaction energy are equal in magnitude, is therefore

$$z_{cn} = \left(\frac{1}{\frac{1}{z_c^3} + \frac{6\pi}{l_m^3}}\right)^{\frac{1}{3}}. \tag{13}$$

Within the short distance of z_{cn}, the top surface of the nanorod affects the motion of the atom approximately in the same way as a large flat surface does. Therefore, we use Eq. (9) to correlate the deflection Δ_f with z_{cn},

$$\Delta_f = \frac{17}{20}\left(\frac{1}{\frac{1}{z_c^3} + \frac{6\pi}{l_m^3}}\right)^{\frac{1}{3}} \tan\theta. \tag{14}$$

In deriving the back deflection Δ_b, we note that the vertical force on the incoming atom dictates the deflection. As the atom is close but not directly above the top surface area in x-y space, the vertical force from one nanorod is the same as ½ of two nanorods symmetrically distributed around the atom, as shown in Fig. 5. As an approximation, the two nanorods of diameter l_m are assumed to interact with the incoming atom in the same way as one nanorod with a cross-sectional area of $\pi l_m^2/2$ that is directly below the atom. The deflection of the atom comes primarily from the short-range interactions, corresponding to Δ_2 of Fig. 2 when the vdW interactions dominate over the initial kinetic energy. Following the same steps in deriving Eq. (7) and Eq. (14), we have

$$\Delta_b = \frac{3}{5}\left(\frac{1}{\frac{2}{z_c^3} + \frac{3\pi}{\sqrt{2}l_m^3}}\right)^{\frac{1}{3}} \tan\theta. \tag{15}$$

Given the front and back deflections in Eq. (14) and Eq. (15), the effective deflection when the incoming atom is on the x-z plane $\Delta = \Delta_f - \Delta_b$ is therefore

$$\Delta = \left[\frac{17}{20}\left(\frac{1}{\frac{1}{z_c^3} + \frac{6\pi}{l_m^3}}\right)^{\frac{1}{3}} - \frac{3}{5}\left(\frac{1}{\frac{2}{z_c^3} + \frac{3\pi}{\sqrt{2}l_m^3}}\right)^{\frac{1}{3}}\right] \tan\theta. \tag{16}$$

Since $l_m \gg z_c$, we approximately have

$$\Delta = \left[\frac{17}{20}\left(1 - \frac{2\pi z_c^3}{l_m^3}\right) - \frac{3}{5}\frac{1}{\sqrt[3]{2}}\left(1 - \frac{\pi z_c^3}{2\sqrt{2}l_m^3}\right)\right] \tan\theta z_c. \tag{17}$$

When the incoming atom is off the x-z plane, we assume that the deflection follows the same expression with l_m replaced by the thickness along the x direction. That is,

$$\Delta(y) = \left[\frac{17}{20}\left(1 - \frac{\pi z_c^3}{4y^3}\right) - \frac{3}{5}\frac{1}{\sqrt[3]{2}}\left(1 - \frac{\pi z_c^3}{16\sqrt{2}y^3}\right)\right] \tan\theta z_c. \tag{18}$$

For a given top surface in Fig. 4, it receives atomic flux from an effective area A_e:

$$A_e = 2\int_0^{x_c} (\Delta(y) + 2y)dx, \tag{19}$$

where x_c is the upper limit where the thickness y along the x direction is equal to z_c; this is to ensure that $l_m \gg z_c$ is valid

at least approximately. Assuming the minimum thickness y_c is equal to z_c, Eq. (19) can be integrated as

$$A_e = \frac{\pi l_m^2}{4}\left\{1+\frac{1}{5}\left[\left(17-\frac{12}{\sqrt[3]{2}}\right)\frac{z_c}{\pi l_m}+\left(\frac{3}{\sqrt[5]{64}}-17\right)\frac{z_c^3}{l_m^3}\right]\tan\theta\right\} \approx \frac{\pi l_m^2}{4}\left\{1+\left[0.48\left(\frac{z_c}{l_m}\right)-3.14\left(\frac{z_c}{l_m}\right)^3\right]\tan\theta\right\}. \quad (20)$$

That is, the effective area is larger than the nominal surface area by a factor f, which is also the ratio of the effective flux F_e on the top surface over the nominal flux F:

$$f = \frac{F_e}{F} = 1+\left[0.48\left(\frac{z_c}{l_m}\right)-3.14\left(\frac{z_c}{l_m}\right)^3\right]\tan\theta. \quad (21)$$

As given in [15], the core diameter of nanorod l_m is given by

$$l_m = \left(\frac{10}{\alpha^2}\ln\frac{n}{2}\frac{v_{3D}}{fF}\right)^{\frac{1}{5}}, \quad (22)$$

where α is the geometrical factor and $\alpha = \pi/4$ for circular cross sections, v_{3D} is the diffusion jump rate of adatoms over multiple-layer surface steps, and n is the number of layers of the nanorod. Typically, $n = 2000$ and its variation does not strongly affect l_m [15]. The two Eqs. (21) and (22) allow the determination of l_m and the factor f. We note that Eq. (22) is valid only when the critical size of nucleation is one or, equivalently, when the product of dimer dissociation time and the number of times a surface site is visited by each adatom is much larger than the time interval between two deposition events on the surface [23]. For typical deposition conditions of Cu nanorod growth—deposition rate of 1.0 nm/s, substrate temperature of 300 K, surface dimension l_m of 15 nm, and dimer binding energy of 0.45 eV [24]—the product is 6.7×10^{-1} s and the time interval is 1.7×10^{-4} s. Since 6.7×10^{-1} is much larger than 1.7×10^{-4}, Eq. (22) is valid under typical conditions of metallic nanorod growth.

As a verification, we have numerically solved the equation of motion with the energy expression of Eq. (10). Based on the relative insensitivity to the kinetic energy as shown in Fig. 3, we choose one kinetic energy of 0.2 eV in the following to verify the closed-form theory of Eq. (21). As Fig. 6(a) shows, the closed-form theory is accurate for all incidence angles as long as the diameter is sufficiently large, i.e., larger than 15 nm. Even for the smaller diameter of 10 nm, the closed-form theory is still accurate as long as the incidence angle is below 88°.

Having verified the closed-form theory in Eq. (21) for the nanorod configuration in Fig. 4, we now extend the verification to a core-shell nanorod. Because the vdW interactions are most effective only at short distances, we expect the theory to be valid. To verify, we have numerically solved the equation of motion of an atom moving toward a core-shell nanorod at different shell angle β, as shown in Fig. 6(b). The numerical results show that this approximation is indeed valid provided that β is below 60°; this condition is satisfied according to our experimental characterizations [15]. So, the interaction with the shell of the nanorod is ignored in the following numerical calculations.

Next, we choose a diameter of 15 nm and verify the theory as a function of the separation of periodic nanorods in hexagonal packing, for various incidence angles. In the numerical solution, we include only the interactions with nanorods within a cutoff distance of 15 nm, for the numerical value of factor f is unchanged even if the cutoff distance is doubled to 30 nm. As Fig. 7(a) shows, the theory is accurate once the separation is sufficiently large. Even for the case of 89°, the difference between the closed-form theory and numerical solutions is within 10%. We note that in reality the separation will be at least as large as the diameter of nanorods, which is about three times that of the core diameter l_m, as the generalized theory shows later in this paper. This means that the separation of nanorods in reality does fall into the range where the theory is accurate. While nanorods can be

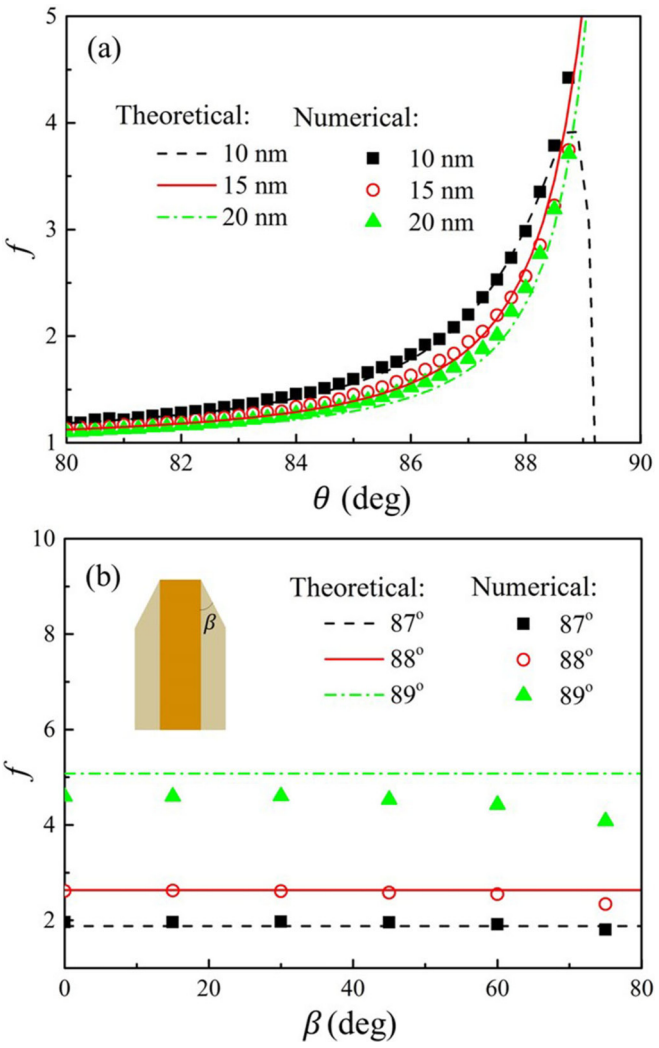

FIG. 6. Comparison of closed-form theory of Eq. (21) with numerical solutions of the equation of motion (a) as a function of angle θ for various diameters of a cylindrical nanorod and (b) as a function of angle β of a core-shell nanorod as shown in the inset, for various incidence angles; $l_m = 15$ nm.

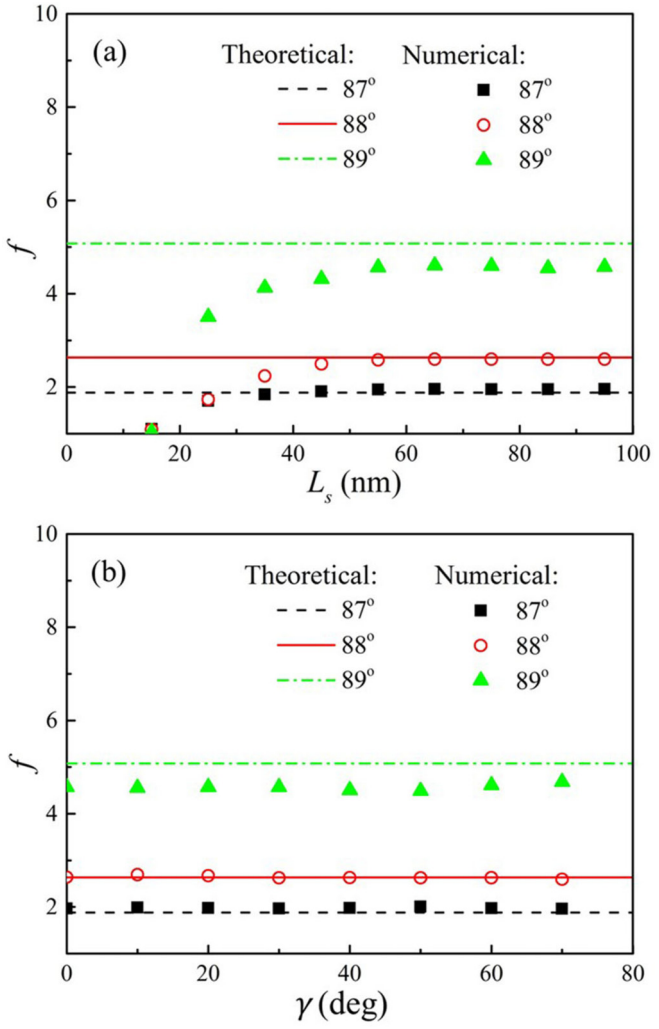

FIG. 7. Comparison of closed-form theory of Eq. (21) with numerical solutions of the equation of motion (a) as a function of separations of hexagonally arranged periodic nanorods for various incidence angles, with $l_m = 15$ nm and (b) as a function of the inclination angle γ of hexagonally arranged periodic nanorods for various incidence angles, with $L_s = 80$ nm and $l_m = 15$ nm.

vertical, as shown in Fig. 1, they often are inclined with an angle γ relative to the substrate normal, as shown in Fig. 8. For inclined nanorods that are in hexagonal packing on a substrate, the numerical solutions verify that the closed-form theory is accurate also; see Fig. 7(b).

Having derived and verified the closed-form theory of factor f, we next derive a generalized theory of nanorod diameter L_m which adds the shell element onto the nanorod core l_m. For periodically arranged nanorods, each nanorod effectively receives the atomic flux of a substrate area A_s. This effective area depends on the separation L_s and how atomic flux arrives. For hexagonally patterned nanorods, which result from glancing angle incidence from the entire 2π range of the azimuthal angle, A_s and L_s are related according to [25]

$$A_s = (\sqrt{3}/2)L_s^2. \tag{23}$$

The rate of deposition in this area, FA_s, has to match the growth rate at the top of nanorod fF over the cross-section

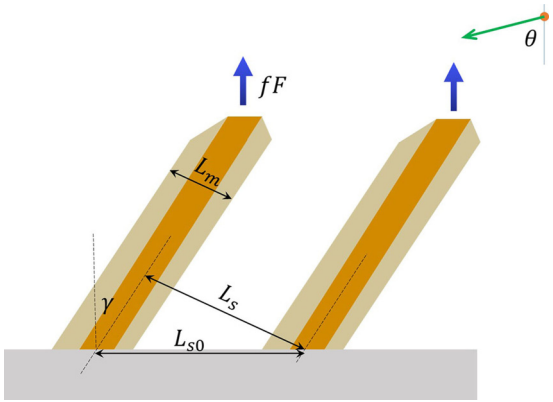

FIG. 8. Schematic of inclined nanorods.

area of the nanorod $(\pi/4)L_m^2$ in order to maintain a quasi-steady-state shape of the nanorod. That is,

$$F\left(\frac{\sqrt{3}}{2}\right)L_s^2 = fF\left(\frac{\pi}{4}\right)L_m^2 \text{ or}$$

$$L_m = \sqrt{\frac{2\sqrt{3}}{\pi f}}L_s. \tag{24}$$

For inclined nanorods (Fig. 8), which result from glancing angle incidence with a fixed azimuthal angle, the thermodynamically preferred top surface, such as {111} for face-centered-cubic metals, is parallel to the substrate [15]. When two nanorods are aligned along the direction of deposition flux, the right nanorod effectively shadows the left. When the two are misaligned, the shadowing is less effective. Our theory corresponds to the most effective shadowing and thereby the smallest diameter. Under the aligned condition, the left nanorod receives atomic flux from an effective area $A_s = L_{s0}L_m$. The rate of deposition in this area, $N = FL_{s0}L_m$, has to match the growth rate at the top of nanorod fF along the vertical direction, or $fF/\cos\gamma$ along the axial direction of the nanorod. Since $L_{s0} = L_s/\cos\gamma$, we have

$$FL_{s0}L_m = \frac{fF}{\cos\gamma}\frac{\pi}{4}L_m^2 \text{ or}$$

$$L_m = \left(\frac{4}{\pi f}\right)L_s. \tag{25}$$

According to Eqs. (24) and (25), L_m linearly scales with L_s. The scaling factor is $\sqrt{f}$ when the incidence flux comes from all possible azimuthal angles, and it is f when the incidence flux comes from one particular azimuthal angle. The numerical factor of order 1 is slightly larger than one because nanorods of circular cross section with $L_m = L_s$ cannot fill all the space. These results are applicable when a quasisteady state is possible—that is, the nanorods will grow taller with the same diameter and shape. For sufficiently small van der Waals interactions, such a quasisteady state is impossible and Eqs. (24) and (25) are no longer valid; our lattice Monte Carlo simulations have verified this impossibility. With the effects of van der Waals interaction, the quasisteady condition is possible when the separation L_s is constant. Due to shadowing and fluctuations of deposition flux over space,

some nanorods lose out, so L_s can change during growth. Consequently, the quasisteady state L_m changes with L_s during growth.

III. EXPERIMENTAL VALIDATION

To validate the closed-form theory, we deposit Cu nanorods using physical vapor deposition. The substrates are Si {100} wafers (Nova Wafers) where the substrate normal is angled at 87, 88, and 89° relative to the deposition flux. A nominal deposition amount for Cu (99.99% Kurt J. Lesker) of 500 nm is used at a rate of 1.0 nm/s, which is determined by a quartz crystal microbalance. Before Cu is deposited, SiO_2 (99.99% KJ Lesker) is deposited on the wafers to a nominal amount of 5 nm at 0.1 nm/s to act as heterogeneous nucleation sites. These depositions are performed in a custom electron-beam physical vapor deposition system with a source to substrate distance of 35 cm. The depositions occur at a vacuum level of $2 \times 10^{-6} \pm 1 \times 10^{-6}$ torr, beginning at 295 K with no substrate temperature control. The substrate temperature increases to 315 K during deposition. Figure 9 shows scanning electron microscopy (SEM, Hitachi S-4800) images of well-separated Cu nanorods deposited at 87, 88, and 89°.

To measure the size and separation of nanorods, SEM images are taken of nanorods from a normal view and from a side view. For each measurement, a pair of nanorods is selected from normal view images by drawing lines along the deposition direction and spacing them to the diameter of a blocking nanorod in front. Two nanorods are close to perfectly aligned when the lines fall on or outside the edges of the second nanorod. Figure 10(a) shows SEM images of the measurements, and compares them to the values used in the theory in Fig. 10(b). The nanorod closer to the deposition source (right) blocks much of the deposition from landing on the side of the second (left) with deposition landing primarily on the top.

The spacing between the nanorods is determined by measuring the distance from one nanorod tip to the second, parallel to the substrate L_{sT}. This is conducted with the image processing tool ImageJ in postprocessing. From this length, the nanorod spacing parallel to the nanorod axis L_s is determined by $L_s = L_{sT} \cos\gamma$. The tip is chosen as the measurement location as it better represents the growth conditions at the end of the deposition and is a clearly defined and visible point in images. Attempts to measure L_{s0} directly results in greater error due to the center line of nanorods at the substrate being difficult to determine from SEM images. As the tip locations in normal images are assumed to be the same height off the substrate, variations in this height can lead to a small difference between the measured L_{sT} and the value of L_{s0}. The resulting error in L_s is determined to be ±15 nm based on the standard deviation of the heights of nanorods. The diameter L_m is

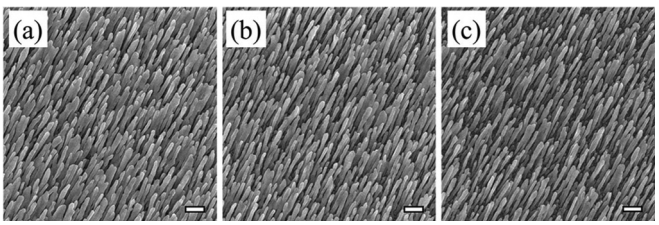

FIG. 9. SEM images of Cu nanorods of 500 nm nominal deposition taken normal to the substrate. The angle of deposition is (a) 87°, (b) 88°, and (c) 89°. The scale bar is 250 nm.

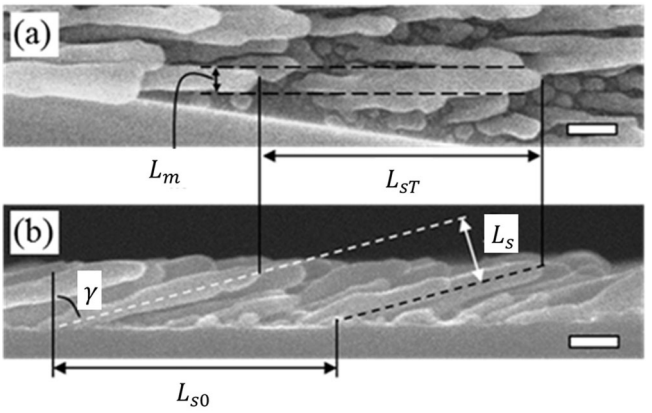

FIG. 10. SEM images of nanorods taken (a) normal to the substrate and (b) from the side, illustrating the measurements L_{sT}, L_m and their relation to L_s, L_{s0}, γ. The scale bar is 100 nm.

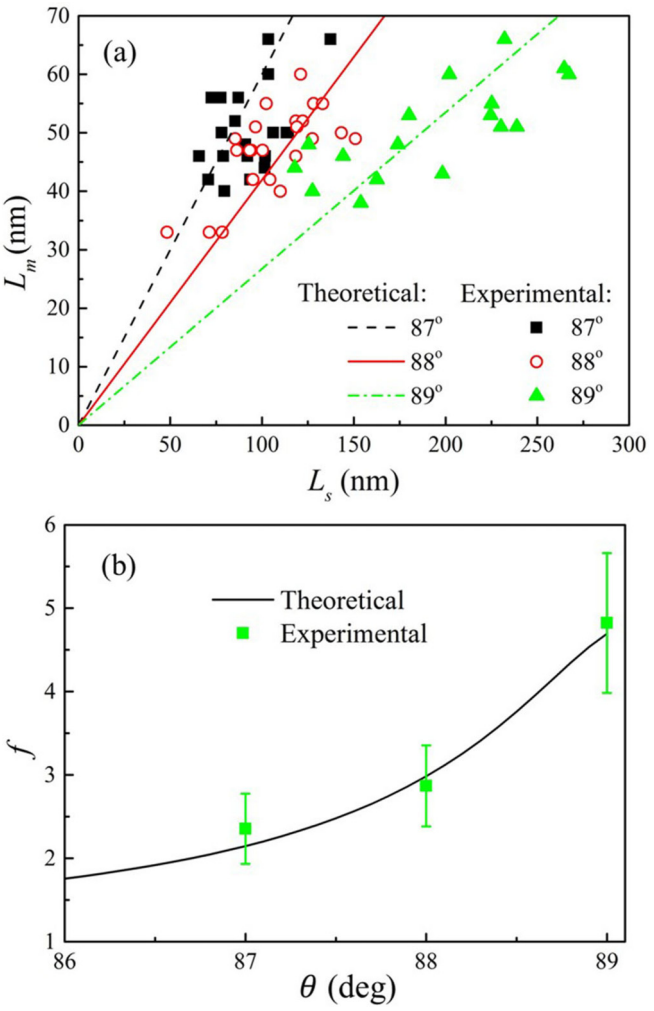

FIG. 11. Comparison of experimental data with closed-form theory for (a) nanorod diameter vs separation and for (b) factor f for three deposition angles.

measured at approximately ¼ of the length from the tip of the nanorod with an error of ±4 nm.

Figure 11(a) shows experimental data of nanorod diameter vs separation under different deposition angles. Based on the theory developed in Ref. [15], the diameter of the nanorod core in Fig. 1 can be determined by including the modification of effective flux given in Eq. (21), which is about 10.8 nm for 87° deposition, 10.9 nm for 88° deposition, and 11.5 nm for 89° deposition. The factor f has a value of about 2.1 for 87° deposition, 3.0 for 88° deposition, and 4.7 for 89° deposition. According to Eq. (25), the diameter of nanorods is related to the separation by $0.60L_s$ for 87° deposition, $0.42L_s$ for 88° deposition, and $0.27L_s$ for 89° deposition. As shown in Fig. 11(a), the experimental results validate the theory of Eq. (25) in terms of linear dependence and slope. Going one step further, we determine the average slope—and thereby the factor f—using the experimental data in Fig. 11(a) and compare it with the theoretical prediction for various incidence angles. As shown in Fig. 11(b), the experimental result and the closed-form theory agree in terms of f. This agreement further confirms the validity of the closed-form theories of the factor f and the diameter L_m.

IV. CONCLUSION

In conclusion, we have reported a generalized theory of nanorod diameter. The generalized theory incorporates non-idealized geometrical shadowing below 90° and incorporates the effects of vdW interactions. To obtain an analytical or closed-form theory, we have made approximations to capture the most important mechanisms. Numerical solutions serve to verify the theory and confirm the reasonableness of the approximations. Further experimental validations serve to show that the closed-form theory can predict the diameter of nanorods in experiments. In contrast to the previous theory for idealized geometrical shadowing [15], the generalized theory predicts nanorod diameters that are a factor of 2 or larger. The theoretical formulations are generic for all metals, and the verification and validation are for copper as one prototype material.

ACKNOWLEDGMENT

The authors gratefully acknowledge the sponsorship of the U.S. Department of Energy Office of Basic Energy Science (Grant No. DE-SC0014035).

[1] C. A. Volkert and E. T. Lilleodden, Philos. Mag. **86**, 5567 (2006).
[2] K. Gall, J. K. Diao, and M. L. Dunn, Nano Lett. **4**, 2431 (2004).
[3] H. S. Park, W. Cai, H. D. Espinosa, and H. C. Huang, MRS Bull. **34**, 178 (2009).
[4] J. D. Driskell, S. Shanmukh, Y. Liu, S. B. Chaney, X. J. Tang, Y. P. Zhao, and R. A. Dluhy, J. Phys. Chem. C **112**, 895 (2008).
[5] Y. J. Liu, H. Y. Chu, and Y. P. Zhao, J. Phys. Chem. C **114**, 8176 (2010).
[6] Y. He, J. Fu, and Y. Zhao, Front. Phys. **9**, 47 (2013).
[7] H. C. Huang, G. H. Gilmer, and T. Díaz de la Rubia, J. Appl. Phys. **84**, 3636 (1998).
[8] H. C. Huang, H. L. Wei, C. H. Woo, and X. X. Zhang, Appl. Phys. Lett. **82**, 4265 (2003).
[9] K. Robbie, M. J. Brett, and A. Lakhtakia, Nature (London) **384**, 616 (1996).
[10] F. Tang, D.-L. Liu, D.-X. Ye, Y.-P. Zhao, T.-M. Lu, and G.-C. Wang, J. Appl. Phys. **93**, 4194 (2003).
[11] M. G. Lagally and Z. Y. Zhang, Nature (London) **417**, 907 (2002).
[12] S. J. Liu, H. C. Huang, and C. H. Woo, Appl. Phys. Lett. **80**, 3295 (2002).
[13] R. L. Schwoebel and E. J. Shipsey, J. Appl. Phys. **37**, 3682 (1966).
[14] G. Ehrlich and F. G. Hudda, J. Chem. Phys. **44**, 1039 (1966).
[15] X. B. Niu, S. P. Stagon, H. C. Huang, J. K. Baldwin, and A. Misra, Phys. Rev. Lett. **110**, 136102 (2013).
[16] Y. Shim, V. Borovikov, and J. G. Amar, Phys. Rev. B **77**, 235423 (2008).
[17] E. Hult, P. Hyldgaard, J. Rossmeisl, and B. I. Lundqvist, Phys. Rev. B **64**, 195414 (2001).
[18] J. F. Annett and P. M. Echenique, Phys. Rev. B **34**, 6853 (1986).
[19] J. G. Amar, Phys. Rev. B **67**, 165425 (2003).
[20] S. van Dijken, L. C. Jorritsma, and B. Poelsema, Phys. Rev. Lett. **82**, 4038 (1999).
[21] S. van Dijken, L. C. Jorritsma, and B. Poelsema, Phys. Rev. B **61**, 14047 (2000).
[22] A. Barranco, A. Borras, A. R. Gonzalez-Elipe, and A. Palmero, Prog. Mater. Sci. **76**, 59 (2016).
[23] J. Krug, P. Politi, and T. Michely, Phys. Rev. B **61**, 14037 (2000).
[24] M. C. Marinica, C. Barreteau, M. C. Desjonqueres, and D. Spanjaard, Phys. Rev. B **70**, 075415 (2004).
[25] L. G. Zhou, and H. C. Huang, Appl. Phys. Lett. **100**, 141605 (2012).